Available online at www.sciencedirect.com
SCIENCE DIRECT®
Journal of Computational Physics 215 (2006) 757–777
JOURNAL OF COMPUTATIONAL PHYSICS
www.elsevier.com/locate/jcp

A splitting moving mesh method for reaction–diffusion equations of quenching type

Kewei Liang [a], Ping Lin [a,*], Ming Tze Ong [b], Roger C.E. Tan [a]

[a] Department of Mathematics, National University of Singapore, Singapore 117543, Singapore
[b] Department of Computational Science, National University of Singapore, Singapore 117543, Singapore

Received 26 January 2005; received in revised form 12 November 2005; accepted 14 November 2005
Available online 28 December 2005

Abstract

This paper studies the numerical solution of multi-dimensional nonlinear degenerate reaction–diffusion differential equations with a singular force term over a rectangular domain. The equations may generate strong quenching singularities. Our work focuses on a variable temporal step Peaceman–Rachford splitting method with an adaptive moving mesh in space. The temporal and spatial adaptation is implemented based on arc-length type of estimations of the time derivative of the solution since the time derivative of the solution approaches infinity when the quenching occurs. The multi-dimensional problem is split into a few one-dimensional problems and the splitting procedure can also be parallelized so that the computational time is significantly reduced. The physical monotonicity of the solution and stability of this variable step moving mesh scheme are analyzed for the time away from the quenching. As stability analysis may not be valid when it is very close to the quenching, thus an exact linear problem is introduced to justify the stability near the quenching time. Finally we provide some numerical examples to illustrate our results as well as to demonstrate the viability and efficiency of the method for the quenching problem or other problems with point singularities. We will also show the significant reduction in computational time required with parallel implementation of the algorithm on a computer with multi-CPU.

MSC: 65K20; 65M50; 35K65; 35B40

Keywords: Nonlinear reaction–diffusion equations; Quenching singularity; Moving mesh method; Peaceman–Rachford splitting; ADI monotonicity; Parallelization

1. Introduction

Many physical phenomena in science and engineering are modeled by partial differential equations with solutions that exhibit localized nonuniformities or singularities in a finite time T. An example is the nonlinear reaction–diffusion equations of quenching type (see e.g. [21,1,9,24]), in which the nonlinear forcing term blows

* Corresponding author. Tel.: +65 68742488; fax: +65 67795452.
E-mail addresses: matlkw@nus.edu.sg (K. Liang), matlinp@nus.edu.sg (P. Lin), sci00056@nus.edu.sg (M.T. Ong), scitance@nus.edu.sg (R.C.E. Tan).

0021-9991/$ - see front matter © 2005 Elsevier Inc. All rights reserved.
doi:10.1016/j.jcp.2005.11.019

up, or the solution quenches and extinguishes, in a finite time when certain environmental parameters exceed their limits at certain special points. Quenching phenomena are distinguished for their important physical phenomenon, superconductive material, engineering interpretations and unique applications in the manufacturing industry.

Finite difference methods have played important roles in solving the above-mentioned partial differential equations numerically. The numerical procedures, however, are often complicated by two facts. One is the strong singularity, such as the rate of the change of the solution blows up at a finite time, developed on relatively small time intervals or spatial length scales. Proper mesh adaptation is necessary to reproduce the singularity. The other is the high dimension which causes tremendous increases in the amount of computations and the complexity of adaptation. Under this circumstance, splitting techniques offer efficient and effective ways to convert higher-dimensional problems into a set of lower-dimensional equations and at the same time offer easy parallelization to largely reduce computational time. It seems to us that such a splitting can be done relatively easier by using the finite difference method.

Considerable efforts have been devoted for computation of quenching solution, or estimates of critical quenching domains of nonlinear reaction–diffusion equations similar to the quenching model (cf. [5,8,16,23,34,11]). Most of them are for one-dimensional problems. Multi-dimensional problems require even much more effort. Most of the existing computations are conducted either based on the reduced problem, that is, the stationary problem by removing the time variable or using uniform temporal and spatial meshes (cf. [9]). Moving mesh approaches have had success for a few blow-up parabolic differential equations [4,5,16,34]. The mesh moving technique is generally well understood for one-dimensional problems but significant challenges remain for multi-dimensional problems (see [12,3,6,7,27,19]). For example, the construction of a moving mesh equation cannot be guided completely by physical arguments. The mesh moving equation is derived based on a minimization of a so-called mesh-energy integral. In higher dimension, it is related to harmonic mapping based methods supplemented with a monitor function to detect the steep transitions in the solution. The high-dimensional monitor function may be tricky to select. The mesh equation may be more complicated than the original equation we want to solve. There are little analysis available about the method due to its difficulty in higher dimensions. These motivate our splitting moving mesh method which is a combination of splitting and mesh-moving. Due to splitting adaptation can always be done in a one-dimensional setting and thus various one-dimensional adaptive techniques can be applied easily and more successfully. The splitting moving mesh procedure can be seen as a special case of general high-dimensional mesh moving techniques. Similar idea such as using tensor-product grid appears recently (see [36]). They have also shown the effectiveness of this type of methods through a few examples. Nevertheless, we may not expect that splitting or tensor-product type of techniques will work for any high-dimensional problems with various singularity patterns (see also a counter example in [36]) if we do not introduce additional transforms or additional treatment. However, due to the point singularity nature of the quenching model the splitting method works well and is very efficient. The parallel implementation is natural and has been done on regular mesh for the splitting procedure. We shall then incorporate it into our splitting moving mesh algorithm. Numerical experiments will demonstrate its good performance on a multi-processor computer.

Physically the solution of the quenching model is monotonically increasing in time. It is important for our finite difference method to preserve this property. In [11] monotonic property is considered for a finite difference scheme under a uniform spatial mesh. In this paper we shall implement our splitting moving mesh method in a way that the idea of proof in [11] can still be used to show the monotonicity of the solution under the (nonuniform) moving spatial mesh. Of course, nonuniform mesh still has to be treated carefully in the analysis. We shall also consider the stability under the variable step moving meshes when it is away from the quenching. When it is near quenching the technique of above analysis is no longer applied. We then introduce an equivalent linear problem to justify the stability of our method. Such theoretical discussion is very difficult for general moving mesh techniques based on minimization of multi-dimensional mesh-energy integral. We shall also show our good computational results and efficiency of our parallel splitting moving mesh algorithm in the last section.

The paper is organized as follows. In Section 2 we will introduce the Peaceman–Rachford splitting method and its combination with moving mesh adaption. We will then analyze the monotonicity of the algorithm in Section 3 and the stability in Section 4. Numerical experiments will be given in Section 5.

2. The quenching model and the adaptive splitting scheme

Let $D = (0, 1) \times (0, 1)$, ∂D be its boundary, and let $\Omega = D \times (0, T)$, $S = \partial D \times (0, T)$ where $0 < T < \infty$. We consider the following degenerate reaction–diffusion problems:

$$\phi(x,y)u_t = \frac{u_{xx}}{a^2} + \frac{u_{yy}}{b^2} + f(u), \quad (x,y,t) \in \Omega, \tag{2.1}$$

$$u(x,y,t) = 0, \ \ (x,y,t) \in S; \quad u(x,y,0) = u_0(x,y), \ \ (x,y) \in D, \tag{2.2}$$

where $\phi(x, y) = (a^2x^2 + b^2y^2)^{q/2}$ $(q \geqslant 0)$. We shall assume that $u_0(x, y) = 0$ which is pretty common for the quenching combustion model and that the source function, $f(u)$, is strictly increasing for $0 \leqslant u < 1$ with

$$f(0) = f_0 > 0, \quad \lim_{u \to 1^-} f(u) = \infty.$$

The model is transformed from that in a general rectangular domain $\{(\tilde{x}, \tilde{y}) \in (0, a) \times (0, b)\}$ by the variable transformation $\tilde{x} = ax$ and $\tilde{y} = by$. In some specific applications (see [2,28]), u represents the temperature in the combustion channel, x and y are coordinates perpendicular and parallel to the channel walls, respectively. The initial temperature $u_0 \geqslant 0$ and is usually very small (it is thus usually assumed to be zero). The function $\phi(x, y)$ represents certain singularity in the temperature transportation speed which causes the degeneracy in the differential equation (2.1) (see [10,15,28] for more details). The solution u of (2.1), (2.2) is said to *quench* if there exists a finite time T such that

$$\sup\{|u_t(x,y,t)| : (x,y) \in \overline{D}\} \to \infty \quad \text{as } t \to T^-. \tag{2.3}$$

The value T is then defined as the *quenching time* [1,2,24]. A necessary condition for quenching to occur is

$$\max\{|u(x,y,t)| : (x,y) \in \overline{D}\} \to 1^- \quad \text{as } t \to T^-. \tag{2.4}$$

It has been shown that such a T exists only when certain spatial references, such as the size of D, reach their critical limits. A domain D^* is called the *critical domain* if the solution of (2.1), (2.2) exists for all time when $D \subseteq D^*$, and (2.4) occurs when $D \supseteq D^*$ for a finite T.

Consider a mesh on the domain $\overline{D}$ with nodes (x_i, y_j), $0 \leqslant i \leqslant I + 1$ and $0 \leqslant j \leqslant J + 1$. We replace the spatial derivatives $u_{xx}(x_i, y_j)$ and $u_{yy}(x_i, y_j)$ by finite differences

$$(u(x_i,y_j))_{\bar{x}\bar{x}} = \left[\frac{u(x_{i+1},y_j) - u(x_i,y_j)}{h_i} - \frac{u(x_i,y_j) - u(x_{i-1},y_j)}{h_{i-1}}\right] \Big/ \bar{h}_i$$

and

$$(u(x_i,y_j))_{\bar{y}\bar{y}} = \left[\frac{u(x_i,y_{j+1}) - u(x_i,y_j)}{k_j} - \frac{u(x_i,y_j) - u(x_i,y_{j-1})}{k_{j-1}}\right] \Big/ \bar{k}_j$$

with $h_i = x_{i+1} - x_i$, $k_j = y_{j+1} - y_j$, $\bar{h}_i = (h_i + h_{i-1})/2$ and $\bar{k}_j = (k_j + k_{j-1})/2$. Let $u_{i,j}(t)$ be an approximation of the solution at the mesh point (x_i, y_j, t), $i = 0, 1, \ldots, I + 1$ and $j = 0, 1, \ldots, J + 1$. Further, let

$$v(t) = (u_{1,1}(t), u_{2,1}(t), \ldots, u_{I,1}(t), \ldots, u_{1,J}(t), \ldots, u_{I,J}(t))^{\mathrm{T}}$$

be the solution and

$$g(v) = (g_{1,1}(t), g_{2,1}(t), \ldots, g_{I,1}(t), \ldots, g_{1,J}(t), \ldots, g_{I,J}(t))^{\mathrm{T}}$$

be the nonhomogeneous term with $g_{i,j}(t) = f(u_{i,j}(t))/\phi(x_i, y_j)$. Removing truncation error terms, we obtain the semi-discretized system

$$v_t(t) = Pv(t) + Rv(t) + g(v(t)), \quad 0 < t < T, \tag{2.5}$$

$$v(0) = v_0, \tag{2.6}$$

where P and R are $IJ \times IJ$ matrices:

$$P = \frac{1}{a^2}\mathrm{diag}(A_j)_{j=1,\cdots,J}, \quad R = \frac{1}{b^2}\tilde{A},$$

$$A_j = \begin{pmatrix} \xi^j_{1,1} & \xi^j_{1,2} & & & & \\ \xi^j_{2,1} & \xi^j_{2,2} & \xi^j_{2,3} & & & \\ & \cdots & \cdots & \cdots & & \\ & & \xi^j_{i,i-1} & \xi^j_{i,i} & \xi^j_{i,i+1} & \\ & & & \cdots & \cdots & \cdots \\ & & & & \xi^j_{I,I-1} & \xi^j_{I,I} \end{pmatrix} \in \mathscr{R}^{I\times I}, \quad \begin{cases} \xi^j_{i,i} = -\frac{2}{h_{i-1}h_i\phi_{i,j}}, \\ \xi^j_{i,i-1} = \frac{1}{h_i h_{i-1}\phi_{i,j}}, \\ \xi^j_{i,i+1} = \frac{1}{h_i h_i \phi_{i,j}}, \end{cases}$$

$$\tilde{A} = \begin{pmatrix} \eta_{1,1}E_1 & \eta_{1,2}E_1 & & & & & \\ \eta_{2,1}E_2 & \eta_{2,2}E_2 & \eta_{2,3}E_2 & & & & \\ & \cdots & \cdots & \cdots & & & \\ & & \eta_{j,j-1}E_j & \eta_{j,j}E_j & \eta_{j,j+1}E_j & & \\ & & & \cdots & \cdots & \cdots & \\ & & & & \eta_{J,J-1}E_J & \eta_{J,J}E_J \end{pmatrix} \in \mathscr{R}^{J\times J},$$

$$\text{where } \begin{cases} \eta_{j,j} = -\frac{2}{k_{j-1}k_j}, \\ \eta_{j,j-1} = \frac{1}{k_j k_{j-1}}, \\ \eta_{j,j+1} = \frac{1}{k_j k_j}, \end{cases} \quad \text{and} \quad E_j = \begin{pmatrix} \frac{1}{\phi_{1,j}} & & & \\ & \frac{1}{\phi_{2,j}} & & \\ & & \cdots & \\ & & & \frac{1}{\phi_{I,j}} \end{pmatrix} \in \mathscr{R}^{I\times I}.$$

We denote $h = \min_i h_i$, $k = \min_j k_j$, $\phi_{\min} = \min_{i,j}\phi_{i,j}$ ($=\phi_{1,1}$ if $q \geqslant 0$). The formal solution of (2.5), (2.6) can thus be written as (preassuming that P and R are not changing with time in a small time interval or within one discrete time step)

$$v(t) = E(tC)v_0 + \int_0^t E((t-\tau)C)g(v(\tau))\mathrm{d}\tau, \quad 0 < t < T,$$

where $E(\cdot) = \exp(\cdot)$ is the matrix exponential and $C = P + R$. In principle, different splitting methods, including ADI and LOD schemes, can be formulated via combinations of a particular numerical quadrature for the integral, together with a proper exponential splitting and an appropriate approximation to E [33]. For example, using a trapezoidal rule for the integral we obtain

$$v(t) \approx E(tC)v_0 + \frac{t}{2}(g(v(t)) + E(tC)g(v_0)). \tag{2.7}$$

Then the Peaceman–Rachford splitting method (cf. [29,32,33]) can be formulated from approximating $E(tC)$ by

$$p(t) = \left(I - \frac{t}{2}R\right)^{-1}\left(I - \frac{t}{2}P\right)^{-1}\left(I + \frac{t}{2}P\right)\left(I + \frac{t}{2}R\right). \tag{2.8}$$

We can easily verify that

$$\|p(t) - E(tC)\|_2 = \mathrm{O}(t^3)$$

in a neighborhood of $t = 0$ (see [32]). So the resulting splitting scheme for the partial differential equation would be of second order accuracy.

Based on (2.7) and (2.8), we obtain the following variable step adaptive Peaceman–Rachford splitting scheme:

$$v_{n+1} = \left(I - \frac{\tau_n}{2}R\right)^{-1}\left(I - \frac{\tau_n}{2}P\right)^{-1}\left(I + \frac{\tau_n}{2}P\right)\left(I + \frac{\tau_n}{2}R\right)\left(v_n + \frac{\tau_n}{2}g(v_n)\right) + \frac{\tau_n}{2}g(v_{n+1}), \tag{2.9}$$

$$\tilde{v}_{n+1} = I_p v_{n+1}, \tag{2.10}$$

where $\tilde{v}_{n+1}$ is the solution defined on the mesh after v_{n+1}, τ_n is the variable temporal step size. $g(v_{n+1})$ in the right hand side of (2.9) may be approximated by $g(w^{(n)})$, where $w^{(n)}$ is an explicit approximation of v_{n+1}, which may be given as

$$w^{(n)} = v_n + \tau_n (v_t)_n = v_n + \tau_n (C v_n + g(v_n)) \tag{2.11}$$

with $C = P + R$. I_p is a matrix associated with a bi-pth order polynomial interpolant, for example (cf. Fig. 2.1),

(i) Bi-linear interpolant:

$$\tilde{v}(X_i, Y_j) = (1-\alpha)(1-\beta)v(x_i, y_j) + \alpha(1-\beta)v(x_{i+1}, y_j) + \alpha\beta v(x_{i+1}, y_{j+1}) + (1-\alpha)\beta v(x_i, y_{j+1}), \tag{2.12}$$

where

$$0 \leqslant \alpha = \frac{X_i - x_i}{h_i} \leqslant 1, \quad 0 \leqslant \beta = \frac{Y_j - y_j}{k_j} \leqslant 1.$$

If (X_i, Y_j) locates in a different rectangular region the definition of α and β may be modified but we can always have $0 \leqslant \alpha \leqslant 1$ and $0 \leqslant \beta \leqslant 1$. Based on the properties of coefficients α and β we see that

$$|\tilde{v}(X_i, Y_j)| \leqslant \max\{|v(x_i, y_j)|, |v(x_{i+1}, y_j)|, |v(x_i, y_{i+1})|, |v(x_{i+1}, y_{j+1})|\}$$

or

$$\|I_1\|_\infty \leqslant 1. \tag{2.13}$$

(ii) Bi-quadratic interpolant:

$$\begin{aligned}\tilde{v}(X_i, Y_j) = {} & (1-\beta_1-\beta_2)(1-\alpha_1-\alpha_2)v(x_{i-1}, y_{j-1}) + (1-\beta_1-\beta_2)\big(\alpha_1 v(x_i, y_{j-1}) + \alpha_2 v(x_{i+1}, y_{j-1})\big) \\ & + \beta_1\big((1-\alpha_1-\alpha_2)v(x_{i-1}, y_j) + \alpha_1 v(x_i, y_j) + \alpha_2 v(x_{i+1}, y_j)\big) \\ & + \beta_2\big((1-\alpha_1-\alpha_2)v(x_{i-1}, y_{j+1}) + \alpha_1 v(x_i, y_{j+1}) + \alpha_2 v(x_{i+1}, y_{j+1})\big),\end{aligned} \tag{2.14}$$

where

$$0 \leqslant \alpha_1 = \frac{(X_i - x_{i-1})(x_{i+1} - X_i)}{h_{i-1}h_i} \leqslant 1, \quad 0 \leqslant \alpha_2 = \frac{(X_i - x_{i-1})(X_i - x_i)}{(h_{i-1} + h_i)h_i} \leqslant 1,$$
$$0 \leqslant \beta_1 = \frac{(Y_j - y_{j-1})(y_{j+1} - Y_j)}{k_{j-1}k_j} \leqslant 1, \quad 0 \leqslant \beta_2 = \frac{(Y_j - y_{j-1})(Y_j - y_j)}{(k_{j-1} + k_j)k_j} \leqslant 1.$$

Noting that

$$1 - \alpha_1 - \alpha_2 = \frac{(X_i - x_i)(X_i - x_{i+1})}{h_{i-1}(h_{i-1} + h_i)} < 0, \quad 1 - \beta_1 - \beta_2 = \frac{(Y_j - y_j)(Y_j - y_{j+1})}{k_{j-1}(k_{j-1} + k_j)} < 0,$$

we generally do not have $\|I_2\|_\infty \leqslant 1$ although the sum of the coefficients is equal to one.

Subsequently our analysis of monotonicity and stability will straightforwardly apply only to the bi-linear interpolation. Nevertheless, numerical experiments indicate that these properties may still hold for bi- quadratic interpolation, especially when the mesh movement is not too dramatic in each step (noting that both

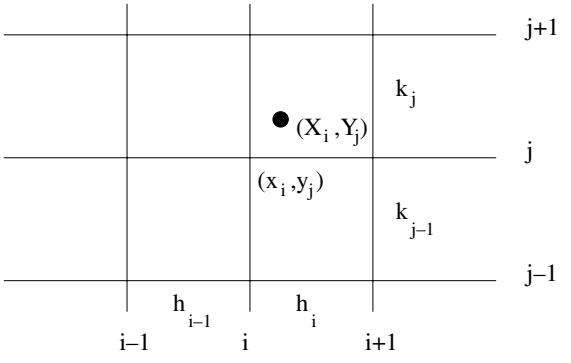

Fig. 2.1. Labeling of points used in the two-dimensional interpolation.

$|1-\alpha_1-\alpha_2|$ and $|1-\beta_1-\beta_2|$ are small if the new mesh point (X_i, Y_j) does not move too far from the previous one (x_i, y_j)). In terms of computational accuracy the bi-quadratic interpolant is a better choice.

The splitting algorithm provides an efficient way for the multi-dimensional computation and significant amount of operations can be saved. Since the strong quenching singularity causes large derivatives in both temporal and spatial directions, it is more efficient to use variable temporal steps τ_n and nonuniform spatial meshes (h_i and k_j) in light of the profile of u_t (see quenching characterization (2.3), (2.4)). We are going to use the one-dimensional moving mesh technique for the spatial mesh and temporal step selection which has largely been studied and has successful application to other combustion and blow-up problems. We shall adopt the following arc-length monitor function on v_t when it is not too large:

$$m(v_t, s) = \sqrt{1+v_{ts}^2}, \quad (x, y, t) \in \Omega, \tag{2.15}$$

where s may be time t or spatial variable x or y. When v_t gets very large the arc-length monitor function may move the spatial mesh too fast and the computational result may not be ideal. Usually, a parameter is introduced to control the spatial mesh, that is, replacing (2.15) for s being x or y by the following:

$$m(v_t, s) = \sqrt{1+\alpha^2 v_{ts}^2}, \quad (x, y, t) \in \Omega. \tag{2.16}$$

We shall choose $\alpha = |v_t|^{-1}$ in our computations and through our numerical experiments this choice of α works well for this quenching model. We would like to remark that other monitor functions may possibly work as well. For example, take the extreme case of (2.16) where α is very large, that is, let $m(v_t, s) = \alpha|v_{ts}|$. Our numerical experience indicates that this derivative monitor function performs well too with a little bit extra mesh moving control. To be more focused in the paper we will simply use the arc-length type of monitor functions (2.15) and (2.16).

We also remark that unlike usual moving mesh PDE techniques our spatial mesh moving strategy is independent of time marching (cf. [18,7,27] for such implementation ideas). Once the spatial mesh at the time $t = t_n$ is done we march to the next time step t_{n+1} with the spatial mesh fixed. Once we have done the time marching we then adjust (move) the mesh within the time step t_{n+1} according to the monitor function (2.16) for spatial variables (cf. Fig. 2.2). We then march to the next time step and so on. Hence, we have the same mesh in each time marching step so that the discussion of monotonicity of the numerical solution in the temporal direction may possibly be carried out more easily. Otherwise the monotonicity property may be much more difficult to achieve. The monotonic increase of the solution in time holds for the continuous quenching model. We shall show later that at every temporal step before quenching the numerical solution is also monotonically increasing if the temporal step size is small enough.

By requiring the maximal arc-lengths in temporal neighboring intervals $[t_{n-2}, t_{n-1}]$ and $[t_{n-1}, t_n]$ be equivalent [12,18,11], we obtain from (2.15) the following equations for τ_n,

$$\tau_n^2 = \tau_{n-1}^2 + ((v_t)_{n-1} - (v_t)_{n-2})^2 - ((v_t)_n - (v_t)_{n-1})^2, \quad n = 2, 3, \ldots, \tag{2.17}$$

with τ_0, τ_1 given. Instead of using sophisticated conventional smoothing processes in standard adaptive algorithms, we choose a minimal temporal step size controller $\tau_{\min}$, $0 < \tau_{\min} \ll \tau_0$, to avoid sudden changes in time marching or any unnecessarily large number of computations near the blow-up of v_t. In spatial directions we

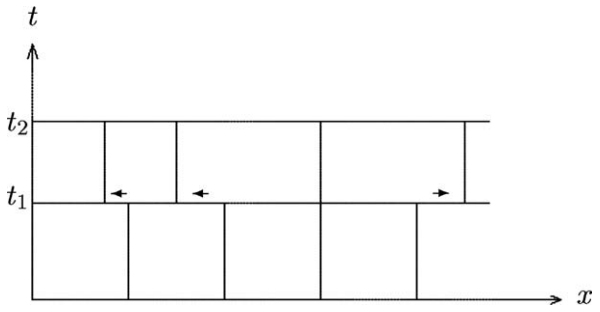

Fig. 2.2. The profile of the mesh in x-direction with moving mesh technique.

shall use equidistribution principle to produce efficient computational meshes. We have no need to design a sophisticated multi-dimensional equidistribution principle since our splitting method splits a multi-dimensional problem to a number of one-dimensional problems. Below we use a conventional one-dimensional equidistribution principle based on the monitor function (2.16):

$$\int_{x_i}^{x_{i+1}} m(u_t,x)\,\mathrm{d}x = \frac{1}{I+1}\int_{x_0}^{x_{I+1}} m(u_t,x)\,\mathrm{d}x, \int_{y_j}^{y_{j+1}} m(u_t,y)\,\mathrm{d}y = \frac{1}{J+1}\int_{y_0}^{y_{J+1}} m(u_t,y)\,\mathrm{d}y,$$

where x_i and y_j are nonuniform mesh points in x and y directions, respectively. For example, along each line $y = y_j$ and starting from the boundary point $(x_{0,j}, y_j)$ on the line we can easily determine $x_{1,j}, \ldots, x_{I,j}$ using above formula, a finite difference approximation for u_{tx} and a numerical integration formula (based on the piecewise linear approximation of u_t). We can then take a new ith x-coordinate x_i^{new} by the following way:

$$x_i^{\text{new}} = x_{i,j_0}, \quad \text{where } j_0 \text{ is an index such that } \max_i |(u_t)_{i,j_0}| = \max_{i,j} |(u_t)_{i,j}|.$$

A new jth y-coordinate $y_j^{\text{new}} = y_{i_0,j}$ can be determined similarly, where $y_{i,0}, y_{i,1}, \ldots, y_{i,J}$ are y-coordinate of mesh points along the line $x = x_i$. If we do not want to move the mesh too much or too little we may implement an average moving strategy. $x_i^{\text{new}} = \frac{1}{J}\sum_{j=1}^{J} x_{i,j}$ and similarly $y_j^{\text{new}} = \frac{1}{I}\sum_{i=1}^{I} y_{i,j}$.

In the next two sections we shall discuss the monotonic increasing property and the stability of the variable step adaptive splitting scheme. Some ideas in [11] for uniform mesh may not work for nonuniform mesh. Also, the nonuniform mesh is moving with the time so both matrices P and R depend on time. We would like to mention here that the time step size selection criterion (2.17) involves the solution at the previous two consecutive time steps. So we shall keep the spatial mesh unchanged during these two consecutive time steps and adapt the temporal step once every two steps for easy implementation.

3. The monotonicity of the discrete solution

The positivity and monotone increasing properties have been characterized as important features of the quenching solutions of nonlinear reaction–diffusion equations such as (2.1), (2.2) (cf. [1,2,9,24]). Thus, it is better to preserve these basic properties in our numerical method. Usually in the quenching model we have $v_0 = 0$. We shall assume $v_0 = 0$ in the discussion of monotonicity in this section.

Lemma 3.1. *If*

$$\frac{\tau_n}{h^2\phi_{\min}} < a^2 \quad \text{and} \quad \frac{\tau_n}{k^2\phi_{\min}} < b^2, \tag{3.18}$$

then matrices

$$I - \frac{\tau_n}{2}P, \quad I - \frac{\tau_n}{2}R, \quad I + \frac{\tau_n}{2}P, \quad \text{and} \quad I + \frac{\tau_n}{2}R$$

are nonsingular. Also, $I - \frac{\tau_n}{2}P$ and $I - \frac{\tau_n}{2}R$ are monotone and inverse-positive. $I + \frac{\tau_n}{2}P$ and $I + \frac{\tau_n}{2}R$ are nonnegative.

Proof. The proof of the lemma is straightforward and can be deduced from the properties of the matrices P and R [11]. □

Lemma 3.2. *If*

$$\frac{\tau_n}{h^2\phi_{\min}} < \frac{1}{2}a^2 \quad \text{and} \quad \frac{\tau_n}{k^2\phi_{\min}} < \frac{1}{2}b^2,$$

then

$$g(0) + \frac{\tau_0^2}{4}PRg(0) > 0.$$

Proof. Denote an IJ-vector

$$\Phi = \left(\phi_{1,1}^{-1}, \phi_{2,1}^{-1}, \ldots, \phi_{I,J}^{-1}\right)^{\mathrm{T}}. \tag{3.19}$$

Noting that $g(0) = f(0)\Phi$ and $f(0) > 0$ (see the assumptions at the beginning of Section 2) we only need to consider $\tilde{\Phi} = \Phi + \frac{\tau_0^2}{4} PR\Phi$. Let $\tilde{\Phi} = (\tilde{\Phi}_{1,1}, \tilde{\Phi}_{2,1}, \ldots, \tilde{\Phi}_{I,J})^{\mathrm{T}}$, where $\tilde{\Phi}_{i,j}$, $1 \leqslant i \leqslant I$ and $1 \leqslant j \leqslant J$, represents the component of the IJ-vector $\tilde{\Phi}$. For $1 < j < J$, we have

$$\begin{aligned}
\tilde{\Phi}_{1,j} &= \phi_{1,j}^{-1} + \frac{\tau_0^2}{4a^2b^2}\left[-\frac{2\phi_{1,j}^{-1}}{h_1h_0}(R\Phi)_{1,j} + \frac{\phi_{1,j}^{-1}}{\bar{h}_1h_1}(R\Phi)_{2,j}\right] \\
&= \phi_{1,j}^{-1} + \frac{\tau_0^2}{4a^2b^2}\left[-\frac{2\phi_{1,j}^{-1}}{h_1h_0}\left(\frac{\phi_{1,j}^{-1}\phi_{1,j-1}^{-1}}{\bar{k}_jk_{j-1}} - \frac{2\phi_{1,j}^{-2}}{k_jk_{j-1}} + \frac{\phi_{1,j}^{-1}\phi_{1,j+1}^{-1}}{\bar{k}_jk_j}\right)\right. \\
&\quad \left. + \frac{\phi_{1,j}^{-1}}{\bar{h}_1h_1}\left(\frac{\phi_{2,j}^{-1}\phi_{2,j-1}^{-1}}{\bar{k}_jk_{j-1}} - \frac{2\phi_{2,j}^{-2}}{k_jk_{j-1}} + \frac{\phi_{2,j}^{-1}\phi_{2,j+1}^{-1}}{\bar{k}_jk_j}\right)\right], \\
\tilde{\Phi}_{i,j} &= \phi_{i,j}^{-1} + \frac{\tau_0^2}{4a^2b^2}\left[\frac{\phi_{i,j}^{-1}}{\bar{h}_ih_{i-1}}(R\Phi)_{i-1,j} - \frac{2\phi_{i,j}^{-1}}{h_ih_{i-1}}(R\Phi)_{i,j} + \frac{\phi_{i,j}^{-1}}{\bar{h}_ih_i}(R\Phi)_{i+1,j}\right] \\
&= \phi_{i,j}^{-1} + \frac{\tau_0^2}{4a^2b^2}\left[\frac{\phi_{i,j}^{-1}}{\bar{h}_ih_{i-1}}\left(\frac{\phi_{i-1,j}^{-1}\phi_{i-1,j-1}^{-1}}{\bar{k}_jk_{j-1}} - \frac{2\phi_{i-1,j}^{-2}}{k_jk_{j-1}} + \frac{\phi_{i-1,j}^{-1}\phi_{i-1,j+1}^{-1}}{\bar{k}_jk_j}\right)\right. \\
&\quad - \frac{2\phi_{i,j}^{-1}}{h_ih_{i-1}}\left(\frac{\phi_{i,j}^{-1}\phi_{i,j-1}^{-1}}{\bar{k}_jk_{j-1}} - \frac{2\phi_{i,j}^{-2}}{k_jk_{j-1}} + \frac{\phi_{i,j}^{-1}\phi_{i,j+1}^{-1}}{\bar{k}_jk_j}\right) + \frac{\phi_{i,j}^{-1}}{\bar{h}_ih_i}\left(\frac{\phi_{i+1,j}^{-1}\phi_{i+1,j-1}^{-1}}{\bar{k}_jk_{j-1}} - \frac{2\phi_{i+1,j}^{-2}}{k_jk_{j-1}} + \frac{\phi_{i+1,j}^{-1}\phi_{i+1,j+1}^{-1}}{\bar{k}_jk_j}\right)\Bigg], \\
\tilde{\Phi}_{I,j} &= \phi_{I,j}^{-1} + \frac{\tau_0^2}{4a^2b^2}\left[\frac{\phi_{I-1,j}^{-1}}{\bar{h}_Ih_{I-1}}(R\Phi)_{I-1,j} - \frac{2\phi_{I,j}^{-1}}{h_Ih_{I-1}}(R\Phi)_{I,j}\right] \\
&= \phi_{I,j}^{-1} + \frac{\tau_0^2}{4a^2b^2}\left[\frac{\phi_{I,j}^{-1}}{\bar{h}_Ih_{I-1}}\left(\frac{\phi_{I-1,j}^{-1}\phi_{I-1,j-1}^{-1}}{\bar{k}_jk_{j-1}} - \frac{2\phi_{I-1,j}^{-2}}{k_jk_{j-1}} + \frac{\phi_{I-1,j}^{-1}\phi_{I-1,j+1}^{-1}}{\bar{k}_jk_j}\right)\right. \\
&\quad \left. - \frac{2\phi_{I,j}^{-1}}{h_Ih_{I-1}}\left(\frac{\phi_{I,j}^{-1}\phi_{I,j-1}^{-1}}{\bar{k}_jk_{j-1}} - \frac{2\phi_{I,j}^{-2}}{k_jk_{j-1}} + \frac{\phi_{I,j}^{-1}\phi_{I,j+1}^{-1}}{\bar{k}_jk_j}\right)\right].
\end{aligned}$$

Similar expressions can be derived for the cases $j = 1$ and $j = J$. Using the condition of the lemma it follows that $\tilde{\Phi}_{i,j} > \frac{5}{8}\phi_{i,j}^{-1} > 0$ which leads to $g(0) + \frac{\tau_0^2}{4} PRg(0) > \frac{5}{8}g(0) > 0$. □

In the next lemma we will show that quenching (i.e., there exists one component of $v_n \geqslant 1$) would not occur at the first time step if τ_0 is small enough.

Lemma 3.3. *If* $\frac{\tau_0}{h^2\phi_{\min}} < a^2$, $\frac{\tau_0}{k^2\phi_{\min}} < b^2$ *and* $h < 1/a\sqrt{2f(0)}$ (*or* $k < 1/b\sqrt{2f(0)}$) *then for given* $v_0 = 0$, *we have that all components of* $v_1 < 1$.

Proof. Let $w = (1, 1, \ldots, 1)^{\mathrm{T}}$. It follows immediately that

$$v_1 = \left(I - \frac{\tau_0}{2}R\right)^{-1}\left(I - \frac{\tau_0}{2}P\right)^{-1}\left(I + \frac{\tau_0}{2}P\right)\left(I + \frac{\tau_0}{2}R\right)\frac{\tau_0}{2}g(0) + \frac{\tau_0}{2}g(\tau_0 g(0))$$

due to the fact that $v_0 = 0$. We further notice that $g(0) = f(0)\Phi$, where Φ is an IJ-vector defined in (3.19). Let $0 < d_0 < 1$ such that $d_0 > \frac{\tau_0 f(0)}{\phi_{\min}}$ (such a d_0 exists due to the assumptions of the lemma), and denote $M = f(d_0)$. Thus, we have $\tau_0 g(0) \leqslant \frac{\tau_0 f(0)}{\phi_{\min}} \leqslant d_0$, and these indicate that

$$g(\tau_0 g(0)) \leqslant g(d_0) = M\Phi.$$

Hence,

$$v_1 - w = \left(I - \frac{\tau_0}{2}R\right)^{-1}\left(I - \frac{\tau_0}{2}P\right)^{-1}\left(I + \frac{\tau_0}{2}P\right)\left(I + \frac{\tau_0}{2}R\right)\frac{\tau_0}{2}g(0) + \frac{\tau_0}{2}g(\tau_0 g(0)) - w$$
$$\leqslant \left(I - \frac{\tau_0}{2}R\right)^{-1}\left(I - \frac{\tau_0}{2}P\right)^{-1} s_1,$$

where

$$s_1 = \frac{\tau_0}{2}\left(I + \frac{\tau_0}{2}P\right)\left(I + \frac{\tau_0}{2}R\right)g(0) + \frac{\tau_0}{2}\left(I - \frac{\tau_0}{2}P\right)\left(I - \frac{\tau_0}{2}R\right)g(d_0) - \left(I - \frac{\tau_0}{2}P\right)\left(I - \frac{\tau_0}{2}R\right)w.$$

In order to see that s_1 is negative, we look into each component of s_1.

From the condition we observe that $\frac{\tau_0}{\phi_{\min}} < a^2h^2$ or b^2k^2. It follows therefore

$$\left|\frac{\tau_0}{2}\left(I + \frac{\tau_0}{2}P\right)\left(I + \frac{\tau_0}{2}R\right)g(0) + \frac{\tau_0}{2}\left(I - \frac{\tau_0}{2}P\right)\left(I - \frac{\tau_0}{2}R\right)g(d_0)\right| \leqslant (f(0) + M)\min\{a^2h^2, b^2k^2\}w.$$

Let the vector

$$\alpha = -\left(I - \frac{\tau_0}{2}P\right)\left(I - \frac{\tau_0}{2}R\right)w = -w + \frac{\tau_0}{2}Cw - \frac{\tau_0^2}{4}PRw.$$

Denote $\alpha = (\alpha_{1,1}, \alpha_{2,1}, \ldots, \alpha_{I,J})^{\mathrm{T}}$, where $\alpha_{i,j}$ is the $(i + (j-1)J)$th component of α. Similarly to the argument in Lemma 3.2, we may show that $\alpha_{i,j} = -1$, for $1 < i < I$ and $1 < j < J$, and $\alpha_{i,j} < -1$ otherwise. This indicates that

$$s < -w + (f(0) + M)\min\{a^2h^2, b^2k^2\}w < -w + 2f(0)\min\{a^2h^2, b^2k^2\}w < 0$$

if $h^2 < 1/2a^2f(0)$ or $k^2 < 1/2b^2f(0)$. This completes the proof. □

The lemma indicates that the solution at the first time step will not quench (i.e., all components of $v_1 < 1$). Our next lemma will indicate that if the solution v_n is before quenching, i.e. all components of $v_n < 1$, and if τ_n is sufficiently small then v_n increases monotonically.

Lemma 3.4. *Let all components of $v_n < 1$ $(n \geqslant 0)$. If $\frac{\tau_n}{h^2\phi_{\min}} < \frac{1}{2}a^2$, $\frac{\tau_n}{k^2\phi_{\min}} < \frac{1}{2}b^2$ and τ_k is sufficiently small for all $n \geqslant 0$ then $v_{n+1} > v_n$ for all $n > 0$ before quenching.*

Proof. Using Lemmas 3.1 and 3.2 and completely following the proof of Lemma 3.6 given in [11] we can obtain the lemma. □

Obviously bi-linear interpolation will keep the monotonicity of the solution sequence v_n, that is, if $v_{n+1} \geqslant v_n$ then $\tilde{v}_{n+1} = I_1 v_{n+1} \geqslant I_1 v_n = \tilde{v}_n$. Combining above results we obtain the following theorem.

Theorem 3.1. *Let $v_0 = 0$. If $\frac{\tau_n}{h^2\phi_{\min}} < \frac{1}{2}a^2$, $\frac{\tau_n}{k^2\phi_{\min}} < \frac{1}{2}b^2$ for all $n \geqslant 0$ and $h < 1/a\sqrt{2f(0)}$ or $k < 1/b\sqrt{2f(0)}$, and if τ_n is sufficiently small then the sequence $\{v_n\}_{n\geqslant 0}$ or $\{\tilde{v}_n\}_{n\geqslant 0}$ produced by the variable step adaptive Peaceman–Rachford splitting (2.9) plus bi-linear interpolation increases monotonically before quenching.*

If we use the bi-quadratic interpolation the corresponding matrix I_2 may have negative element which may affect the monotonicity. Nevertheless, our numerical results indicate that the monotonicity in time still holds within the range of accuracy. Theoretically we may possibly construct monotonicity-preserving interpolation (cf. [22]), which usually involves polynomial interpolations of higher degree.

4. Stability

Stability of the splitting has been a difficult issue when solving nonlinear blow-up type or quenching type problems, especially when using variable time steps and nonuniform meshes. Most analysis of the Peaceman–Rachford splitting or its variants is conducted for uniform time steps and uniform spatial meshes (cf. [13]). In [35,32] variable time steps may be included in stability analysis but a certain kind of commutative condition of two splitting operators or matrices has to be assumed. In [20] a variant of the Peaceman–Rachford splitting is analyzed and commutative condition may be removed but uniform time step is assumed. A one-sided Lipschitz condition is also assumed in [20]. In [11] the stability of the variable step splitting scheme (2.9)

on a uniform spatial mesh is analyzed with the nonlinear term frozen. In this section, we will do the analysis for variable time steps on a nonuniform spatial mesh. We will freeze the source term g first. Freezing the source term g is equivalent to assuming that it does not depend on the solution. As far as the stability is concerned, this is equivalent to setting g as zero. In other words, we only establish the stability of the discretization of $(u_{xx}+u_{yy})/\phi(x,y)$. When we include a linearized g in the analysis then this linear part of g might dominate the Laplacian term near the quenching time and then the stability analysis done from assuming $g(v)$ frozen is no longer apply near the quenching time. We then consider an exact linearized model and use it to justify the stability near the quenching time. Our numerical experiments demonstrate that the scheme is indeed stable even if it is near the quenching time.

4.1. Stability away from quenching

We consider in this subsection the stability for the variable step adaptive Peaceman–Rachford method (2.9). We will first frozen the nonlinear term $g(v)$. Then we will remark the case where $g(v)$ varies.

Theorem 4.1. *Let*

$$\frac{\tau_\ell}{h^2\phi_{\min}}<\frac{1}{2}a^2,\quad \frac{\tau_\ell}{k^2\phi_{\min}}<\frac{1}{2}b^2, \tag{4.20}$$

and τ_ℓ be sufficiently small for all $0\leqslant \ell\leqslant n$. Then the variable step adaptive Peaceman–Rachford method (2.9) plus the bi-linear interpolation (with the nonlinear term frozen) is stable in the sense of the maximum norm, i.e.,

$$\|z_{n+1}\|_\infty \leqslant c_{h,k}\|z_0\|_\infty,$$

where $z_0=v_0-\bar{v}_0$ is an initial perturbation or error, $z_\ell=v_\ell-\bar{v}_\ell$ $(0\leqslant\ell\leqslant n+1)$ is the perturbation arising from the initial perturbation z_0, and $c_{h,k}$ is a positive constant independent of the number of time steps n and of the time step sizes τ_ℓ $(0\leqslant\ell\leqslant n)$.

Proof. Since the nonlinear term is frozen (i.e., $g(v)$ is treated as a constant) the perturbation $z_{\ell+1}$ satisfies

$$z_{\ell+1}=I_1\Big(I-\frac{\tau_\ell}{2}R_\ell\Big)^{-1}\Big(I-\frac{\tau_\ell}{2}P_\ell\Big)^{-1}\Big(I+\frac{\tau_\ell}{2}P_\ell\Big)\Big(I+\frac{\tau_\ell}{2}R_\ell\Big)z_\ell. \tag{4.21}$$

Under the assumption (4.20) the sum of the absolute value of entries in each row of $I+\frac{\tau_\ell}{2}P$ and $I+\frac{\tau_\ell}{2}R$ is less than or equal to one. That is

$$\Big\|I+\frac{\tau_\ell}{2}P\Big\|_\infty\leqslant 1\quad\text{and}\quad\Big\|I+\frac{\tau_\ell}{2}R\Big\|_\infty\leqslant 1. \tag{4.22}$$

Furthermore, we have $\|\frac{\tau_\ell}{2}P\|_\infty<1$ due to the assumption (4.20). When τ_ℓ is sufficiently small, we can easily obtain

$$\Big(I-\frac{\tau_\ell}{2}P\Big)^{-1}=I+\frac{\tau_\ell}{2}P+\Big(\frac{\tau_\ell}{2}P\Big)^2+\cdots$$

and a similar expansion for $\big(I-\frac{\tau_\ell}{2}R\big)^{-1}$. Therefore,

$$\Big\|\Big(I-\frac{\tau_\ell}{2}P\Big)^{-1}\Big\|_\infty\leqslant 1+O_{h,k}(\tau_\ell^2)\quad\text{and}\quad\Big\|\Big(I-\frac{\tau_\ell}{2}R\Big)^{-1}\Big\|_\infty\leqslant 1+O_{h,k}(\tau_\ell^2). \tag{4.23}$$

Using (2.13), (4.22) and (4.23) in (4.21), we then obtain

$$\begin{aligned}\|z_{n+1}\|_\infty&\leqslant(1+O_{h,k}(\tau_n^2))\|z_n\|_\infty\leqslant\cdots\leqslant(1+O_{h,k}(\tau_n^2))\cdots(1+O_{h,k}(\tau_0^2))\|z_0\|_\infty\\&\leqslant\big(1+O_{h,k}(\tau_n^2+\tau_{n-1}^2+\ldots+\tau_0^2)\big)\|z_0\|_\infty\leqslant c_{h,k}\|z_0\|_\infty.\qquad\square\end{aligned} \tag{4.24}$$

From the proof we can see that if τ_ℓ $(0\leqslant\ell\leqslant n)$ are sufficiently small we may have $c_{h,k}<2$.

Remark 4.1. In the case that $g(v)$ varies we will have the following linearized relation:

$$z_{\ell+1}=I_1\Big[\Big(I-\frac{\tau_\ell}{2}R_\ell\Big)^{-1}\Big(I-\frac{\tau_\ell}{2}P_\ell\Big)^{-1}\Big(I+\frac{\tau_\ell}{2}P_\ell\Big)\Big(I+\frac{\tau_\ell}{2}R_\ell\Big)\Big(z_\ell+\frac{\tau_\ell}{2}g_v z_\ell\Big)+\frac{\tau_\ell}{2}(z_\ell+\tau_\ell(C_\ell z_\ell+g_v z_\ell))\Big].$$

We notice that there is at least a τ_ℓ factor associated with extra terms arising from varied $g(v)$. So we expect that the stability still holds if it is away from quenching, i.e. v is away from one. When v approaches one g_v tends to infinity and the situation is not clear. Conjectured in [25] and shown for one-dimensional cases in [17,14] that $1-u$ is proportional to $(T-t)^{\frac{1}{1+\theta}}$ when $q=0$ and $f(u)=(1-u)^{-\theta}$, where T is the quenching time. This conjecture of quenching rate is also demonstrated by our numerical experiments in Section 5. For this $f(u)$ and $q=0$, $g_v=\theta(1-u)^{-(\theta+1)}$ is proportional to $(T-t)^{-1}$. Therefore, $\tau_\ell g_v$ would not be small as t is close to the quenching time T. The argument used in the proof of Theorem 4.1 may not be valid.

4.2. Stability near the quenching time

We would like to consider how the discrete solution behaves near the quenching time. As we mentioned above near the quenching $\tau_\ell g_v$ need not be very small and the stability analysis conducted earlier is no longer valid. So we look for alternative ways to justify the stability. To avoid technical difficulties of our stability justification we shall fix the nonuniform spatial mesh and study the semi-discrete difference scheme (2.5) and the splitting scheme (2.9). To further simplify the discussion we shall also assume that $f(u)=1/(1-u)^\theta$ ($\theta>0$), which is a usual choice of $f(u)$ among quenching models discussed by other researchers (see e.g. [21,9,24,1]). The discussion in this section does not intend to provide a rigorous proof but to provide a justification of the stability near the quenching time for the adaptive splitting algorithm (2.9), (2.10). We first write the differential equation (2.1) to a mathematically equivalent linear form

$$u_t=\frac{1}{a^2\phi}u_{xx}+\frac{1}{b^2\phi}u_{yy}+\frac{1}{\phi(1-u_e)^{\theta+1}}(1-u), \tag{4.25}$$

where $u_e(x,y,t)$ is the exact solution of (2.1), (2.2). So the solution of (4.25), (2.2) is the same as that of (2.1), (2.2) due to the uniqueness of the solution (which can be deduced from the maximum principle [30]). It can also be shown from the maximum principle that $0\leqslant u_e<1$ and u_e increases in t. The semi-discretized scheme (2.5) (in the component-wise form) of (4.25) reads

$$(u_{i,j})_t=(u_{i,j})_{\bar{x}\hat{x}}+(u_{i,j})_{\bar{y}\hat{y}}+\frac{1}{(1-(u_e)_{i,j}(t))^{\theta+1}}(1-u_{i,j}) \tag{4.26}$$

satisfying boundary condition (2.2) and initial condition $u_{i,j}(t_\delta)=u^d_{i,j}(t_\delta)$, where $t_\delta=T-\delta$ ($t_\delta\leqslant t<T$ is a neighborhood of the quenching time T) and u^d represents the solution of (4.26) with boundary and initial conditions (2.2).

Lemma 4.1 (Discrete maximum principle). *If* $w_{i,j}(t)(L_0+\gamma_{i,j}(t))\geqslant 0$ ($\gamma\geqslant 0$), *where*

$$L_0w_{i,j}=(w_{i,j})_t-\frac{1}{a^2\phi_{i,j}}(w_{i,j})_{\bar{x}\hat{x}}-\frac{1}{b^2\phi_{i,j}}(w_{i,j})_{\bar{y}\hat{y}},\quad \phi_{i,j}>0,$$

$w_{i,j}|_{t=t_\delta}\geqslant 0$ *for all nodes* (i,j) *in* D, *and* $w_{i,j}\geqslant 0$ *for all the boundary nodes in* ∂D, *then* $w_{i,j}\geqslant 0$ *holds for all* t ($T>t>t_\delta$) *and all nodes* (i,j) *in* D.

Proof. The idea of proof may be found in many standard text books, for example [30]. Assume that the conclusion is false; then there is a first $\tilde{t}>t_\delta$ such that $w_{i,j}(\tilde{t})<0$ for some $(\tilde{i},\tilde{j})$ in the domain D, $w_{i,j}\geqslant 0$ for $t\in[t_\delta,\tilde{t})$ and $(i,j)\in\overline{D}$, and $(w_{\tilde{i},\tilde{j}})_t(\tilde{t})\leqslant 0$. Moreover, we can assume that $w_{i,j}(\tilde{t})$ attains its minimum at $(i,j)=(\tilde{i},\tilde{j})$ and that there is at least one neighbor (i_b,j_b) of $(\tilde{i},\tilde{j})$[1] such that $w_{i_b,j_b}(\tilde{t})$ is strictly less than $w_{\tilde{i},\tilde{j}}(\tilde{t})$. We then have that $(w_{\tilde{i},\tilde{j}}(\tilde{t}))_{\bar{x}\hat{x}}+(w_{\tilde{i},\tilde{j}}(\tilde{t}))_{\bar{x}\hat{x}}$ is positive. Hence, $(L_0+\gamma_{\tilde{i},\tilde{j}})w_{\tilde{i},\tilde{j}}(\tilde{t})<0$, which, however, is a contradiction. □

[1] The neighbors of (i,j) is defined at the nodes: $(i-1,j)$, $(i,j-1)$, $(i+1,j)$ and $(i,j+1)$.

Now we introduce a perturbation $z_{i,j}(t_\delta) = u_{i,j}(t_\delta) - \bar{u}_{i,j}(t_\delta)$ at the time $t = t_\delta$, where $u_{i,j}(t)$ is the solution of (4.26) and $\bar{u}_{i,j}(t)$ is the perturbed solution due to the initial perturbation $z_{i,j}(t_\delta)$. Then the perturbation $z_{i,j}(t)$ satisfies the following perturbation equation:

$$(z_{i,j})_t = \frac{1}{a^2\phi_{i,j}}(z_{i,j})_{\bar{x}\hat{x}} + \frac{1}{b^2\phi_{i,j}}(z_{i,j})_{\bar{y}\hat{y}} - \frac{1}{\phi_{i,j}(1-(u_e)_{i,j}(t))^{\theta+1}} z_{i,j} \tag{4.27}$$

with boundary condition $z_{i,j} = 0$ for all boundary nodes (i, j) in ∂D. We can then construct a barrier function $Z_{i,j}(t) = \max_{i,j} |z_{i,j}(t_\delta)| \pm z_{i,j}(t)$.

Then it is not difficult to verify that

$$\left(L_0 + \frac{1}{\phi_{i,j}(1-(u_e)_{i,j}(t))^{\theta+1}}\right) Z_{i,j}(t) = \frac{1}{\phi_{i,j}(1-(u_e)_{i,j}(t))^{\theta+1}} \max_{i,j} |z_{i,j}(t_\delta)| > 0.$$

and $Z_{i,j}(t_\delta) \geqslant 0$ for nodes (i, j) in D and $Z_{i,j}(t) \geqslant 0$ for all boundary nodes (i, j) in ∂D. From the discrete maximum principle we thus have $Z_{i,j}(t) \geqslant 0$ for all nodes (i, j) in D and all t ($T > t > t_\delta$). We then obtain a stability estimate for the semi-discretized problem (2.5)

$$|z_{i,j}(t)| \leqslant \max_{i,j} |z_{i,j}(t_\delta)| \tag{4.28}$$

for $T > t \geqslant t_\delta$ and all nodes (i, j) in D.

Next we consider the stability for the Peaceman–Rachford splitting scheme (2.9) applied to the exact linearized problem (4.25) near quenching. Define the perturbation $z_\ell = (\ldots z_{i,j}^\ell \ldots)$ at the time level $t = t_\ell$ as in (4.21) and $\gamma_{i,j}(t) = \frac{1}{\phi_{i,j}(1-(u_e)_{i,j}(t))^{\theta+1}} > 0$. Then

$$z_{\ell+1} = \left(I - \frac{\tau_\ell}{2}R\right)^{-1}\left(I - \frac{\tau_\ell}{2}P\right)^{-1}\left(I + \frac{\tau_\ell}{2}P\right)\left(I + \frac{\tau_\ell}{2}R\right)\left(z_\ell - \frac{\tau_\ell}{2}\Gamma_\ell z_\ell\right) - \frac{\tau_\ell}{2}\Gamma_{\ell+1}z_{\ell+1}, \tag{4.29}$$

where $\Gamma_\ell = \mathrm{diag}(\ldots\gamma_{i,j}(t_\ell)\ \ldots)$ is a diagonal matrix. Hence

$$\begin{aligned}
z_{\ell+1} &= \left(I + \frac{\tau_\ell}{2}\Gamma_{\ell+1}\right)^{-1}\left(I - \frac{\tau_\ell}{2}R\right)^{-1}\left(I - \frac{\tau_\ell}{2}P\right)^{-1}\left(I + \frac{\tau_\ell}{2}P\right)\left(I + \frac{\tau_\ell}{2}R\right)\left(I - \frac{\tau_\ell}{2}\Gamma_\ell\right)z_\ell \\
&= \left(I + \frac{\tau_\ell}{2}\Gamma_{\ell+1}\right)^{-1}\left(I - \frac{\tau_\ell}{2}R\right)^{-1}\left(I - \frac{\tau_\ell}{2}P\right)^{-1}\left(I + \frac{\tau_\ell}{2}P\right)\left(I + \frac{\tau_\ell}{2}R\right)\left(I - \frac{\tau_\ell}{2}\Gamma_\ell\right)\left(I + \frac{\tau_{\ell-1}}{2}\Gamma_\ell\right)^{-1} \\
&\quad \times \left(I - \frac{\tau_{\ell-1}}{2}R\right)^{-1}\left(I - \frac{\tau_{\ell-1}}{2}P\right)^{-1}\left(I + \frac{\tau_{\ell-1}}{2}P\right)\left(I + \frac{\tau_{\ell-1}}{2}R\right)\left(I - \frac{\tau_{\ell-1}}{2}\Gamma_{\ell-1}\right)\left(I + \frac{\tau_{\ell-2}}{2}\Gamma_{\ell-1}\right)^{-1} \\
&\quad \cdots \left(I + \frac{\tau_{\ell_0}}{2}\Gamma_{\ell_0+1}\right)^{-1}\left(I - \frac{\tau_{\ell_0}}{2}R\right)^{-1}\left(I - \frac{\tau_{\ell_0}}{2}P\right)^{-1}\left(I + \frac{\tau_{\ell_0}}{2}P\right)\left(I + \frac{\tau_{\ell_0}}{2}R\right)\left(I - \frac{\tau_{\ell_0}}{2}\Gamma_{\ell_0}\right)z_{\ell_0},
\end{aligned}$$

where ℓ_0 is the beginning step, i.e. $t_{\ell_0} = t_\delta$. We only need to estimate

$$A = \left\| \left(I - \frac{\tau_\ell}{2}\Gamma_\ell\right)\left(I + \frac{\tau_{\ell-1}}{2}\Gamma_\ell\right)^{-1}\left(I - \frac{\tau_{\ell-1}}{2}\Gamma_{\ell-1}\right)\left(I + \frac{\tau_{\ell-2}}{2}\Gamma_{\ell-1}\right)^{-1} \cdots \left(I - \frac{\tau_{\ell_0+1}}{2}\Gamma_{\ell_0+1}\right)\left(I + \frac{\tau_{\ell_0}}{2}\Gamma_{\ell_0+1}\right)^{-1} \right\|_\infty \tag{4.30}$$

since other matrix factors can be estimated similarly to the proof of Theorem 4.1 preassuming that all the conditions of Theorem 4.1 hold. When it is near quenching $(u_{i,j})_t$ should be very large and we expect that the minimal time step (say, $\tau_{\min}$) has been reached. So we may assume $\tau_\ell = \tau_{\min}$ for all near-quenching steps ℓ. Hence

$$\begin{aligned}
&\left\| \left(I - \frac{\tau_\ell}{2}\Gamma_\ell\right)\left(I + \frac{\tau_{\ell-1}}{2}\Gamma_\ell\right)^{-1} \right\|_\infty = \max_{i,j} \frac{|1 - \frac{\tau_{\min}}{2}\gamma_{i,j}(t_\ell)|}{|1 + \frac{\tau_{\min}}{2}\gamma_{i,j}(t_\ell)|} < 1, \\
&\left\| \left(I - \frac{\tau_{\ell-1}}{2}\Gamma_{\ell-1}\right)\left(I + \frac{\tau_{\ell-2}}{2}\Gamma_{\ell-1}\right)^{-1} \right\|_\infty = \max_{i,j} \frac{|1 - \frac{\tau_{\min}}{2}\gamma_{i,j}(t_{\ell-1})|}{|1 + \frac{\tau_{\min}}{2}\gamma_{i,j}(t_{\ell-1})|} < 1, \\
&\cdots\cdots \\
&\left\| \left(I - \frac{\tau_{\ell_0+1}}{2}\Gamma_{\ell_0+1}\right)\left(I + \frac{\tau_{\ell_0}}{2}\Gamma_{\ell_0+1}\right)^{-1} \right\|_\infty = \max_{i,j} \frac{|1 - \frac{\tau_{\min}}{2}\gamma_{i,j}(t_{\ell_0+1})|}{|1 + \frac{\tau_{\min}}{2}\gamma_{i,j}(t_{\ell_0+1})|} < 1.
\end{aligned}$$

So if all conditions of Theorem 4.1 hold then we have

$$\|z_{\ell+1}\|_\infty \leqslant c_{h,k}\|z_{\ell_0}\|_\infty \tag{4.31}$$

for all ℓ near the quenching.

5. Parallel implementation and numerical experiments

5.1. Parallel implementation

At each time step the splitting procedure can be easily parallelized as having been done by many people usually on a uniform mesh. It is not difficult to incorporate the moving mesh into the parallel implementation. We have carried out the parallel computation using open MP on an IBM p690 with shared memory. The Peaceman–Rachford splitting (2.9), (2.10) can be divided into four stages:

$$\begin{aligned}
&\text{(I)}\quad S_1 = \left(I + \frac{\tau_n}{2}R\right)\left(v_n + \frac{\tau_n}{2}g(v_n)\right),\\
&\text{(II)}\quad S_2 = (I - \frac{\tau_n}{2}P)^{-1}(I + \frac{\tau_n}{2}P)S_1,\\
&\text{(III)}\quad S_3 = (I - \frac{\tau_n}{2}R)^{-1}S_2 + \frac{\tau_n}{2}g(w^{(n)}),\\
&\text{(IV)}\quad v_{n+1} = I_p S_3,
\end{aligned}$$

where each stage involves with a number of one-dimensional implementation. In stage (II) we solve a one-dimension (tridiagonal) linear system at each grid line $y = y_j$ $(1 \leqslant j \leqslant J)$ and in stage (III) we solve a one-dimension (tridiagonal) linear system at each grid line $x = x_i$ $(1 \leqslant i \leqslant I)$. The computation at one grid line is independent of that at other grid lines and thus can be done simultaneously by assigning it to a number of processors. So if we have m processors then in the x direction and y direction each processor is responsible for solving J/m sets and I/m sets of tridiagonal systems respectively, as opposed to one processor solving all J and I sets of tridiagonal systems. This parallel implementation would largely reduce the computational time. Once we complete sweeps along both x and y directions we can then move the mesh in both x and y directions and use the bi-linear or bi-quadratic interpolation to obtain v_{n+1} in stage (IV). Fig. 5.1 shows the reduction in computational time when a number of processors are used to solve (2.1), (2.2) with $a = b = 3$ and under an 81×81 grid.

5.2. Computational experiments

In this subsection we present numerical experiments for two-dimensional examples, such as classical quenching problem, degenerate quenching problem and a vortex model of superconductor. Throughout the numerical results we always adopt $N = 41 \times 41$ grid points in the splitting moving mesh method unless otherwise stated. And the quenching time is determined by the criterion $u > 1 - \tau_{\min}$.

Example 5.2.1. Let $\theta > 0$ and $D = (0,a) \times (0,b)$. We first compute the critical domain of the following classical quenching problem (which is equivalent to (2.1), (2.2) with $q = 0$, i.e. $\phi(x, y) \equiv 1$)

$$u_t = u_{xx} + u_{yy} + \frac{1}{(1-u)^\theta}, \quad (x,y) \in D,\ 0 < t < T, \tag{5.32}$$

$$u(x,y,0) = 0, \quad (x,y) \in D; \tag{5.33}$$

$$u(0,y,t) = u(a,y,t) = u(x,0,t) = u(x,b,t) = 0,\ 0 < t < T. \tag{5.34}$$

Our goal is to predict the critical sizes of the domain. The authors of [9,11] have investigated these in different ratio of a and b with $\theta = 1$. Their results were well matched except the case of ratio $a/b = 1$ (see [11]; Table 5.1).

For the case of $a = b$, we list, in Table 5.1, our newly computed results together with the existing results for a comparison. D_a is the critical size of the domain estimated in [9], D_b is the critical size obtained in [11] with uniform grid points 81×81, and D_c is our result with adaptive grid points $N = 41 \times 41$, initial temporal step

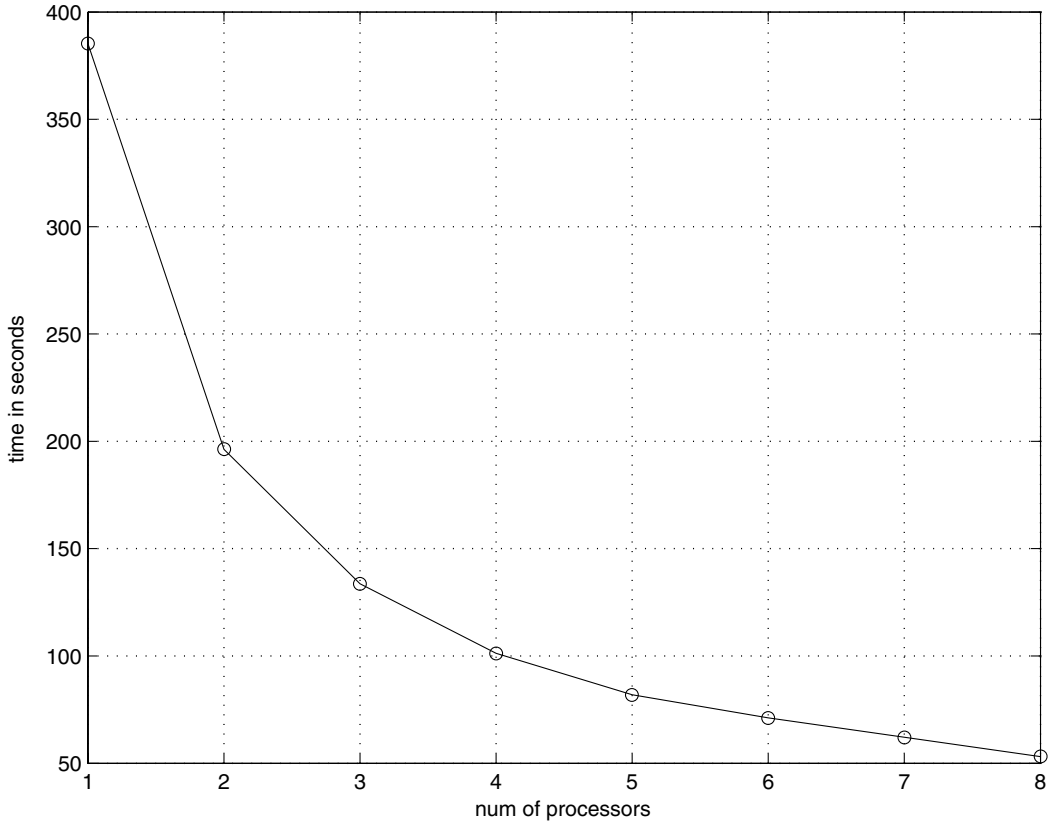

Fig. 5.1. Computational time vs. number of processors.

Table 5.1
A comparison of our numerical prediction with existing result given in [9,11] when Ratio $a/b = 1$ and $\theta = 1$. D_a, D_b and D_c are, respectively, areas of the critical domain in [9,11] and newly computed critical domain (obtained by our adaptive method)

Ratio a/b	D_a	D_b	D_c
1.000	4.45375	4.49606	4.45398

$\tau_0 = 10^{-3}$ and minimal temporal controller $\tau_{\min} = 10^{-4}$. (We can take $\tau_{\min}$ smaller and the result is similar in this case.) We note that even though we take fewer spatial grids and bigger temporal step size than [11] where the uniform mesh is used, our approximate critical size is closer to that predicted in [9] than [11].

In Table 5.2, we present the corresponding quenching times for the different size of the domain D between D_b and D_c when the ratio of a/b is 1. The first two columns of Table 5.2 shows that if the domain size D has a small fluctuation from 4.496062 to 4.496058 ($\Delta D = 4.496062 - 4.496058 = 4.0 \times 10^{-6}$), the corresponding quenching time may have a big change ($|\Delta T| = |5.725654 - 5.725954| = 3.0 \times 10^{-4}$). This shows the sensitivity

Table 5.2
The quenching times for different domain sizes between D_b and D_c obtained via the splitting moving mesh method when the ratio $a/b = 1$ and $\theta = 1$. The number of spatial grids and initial temporal step size as well as minimal temporal controller are the same as those in Table 5.1

a	2.120392	2.120391	2.110500	2.110451	2.110450	2.110446	2.110445
D	4.496062 (D_b)	4.496058	4.454210	4.454003	4.453999	4.453982	4.453978 (D_c)
T	5.725654	5.725954	80.724993	225.954099	243.456150	407.393949	548.994850

of the quenching times to the choice of the domain sizes. The closer the domain size approaches the critical size, the more serious the sensitivity is. From 4.454003 to 4.453999, $\Delta D = 4.454003 - 4.453999 = 4.0 \times 10^{-6}$ is the same as before, whereas $|\Delta T| = |225.954099 - 243.456150| = 17.502051$. When the size changes from 4.453982 to 4.453978, $|\Delta T| = |407.393949 - 548.994850| = 141.600901$.

Fig. 5.2 shows the evolution of the function u in main graphs and its derivative u_t in sub-graphs for problem (5.32), (5.34) with $\theta = 1$. The domain parameter $a = 3.0$ with ratio $a/b = 1$ is used. The four different stages of u and u_t, that is, $t = 0.3$, 0.6, 0.616402 and 0.61697 are displayed. Moreover, from the left profile of Fig. 5.4, it can be observed that the peak of u_t has reached 185.37580 when $t = 0.61697$. Further, Fig. 5.3 shows the spatial adaptive mesh immediately before quenching at $t = 0.61697$ for the problem (5.32), (5.34) with $a = 3.0$, $a/b = 1$ and $\theta = 1$. The close-up look of the central part of the adaptive mesh is depicted in the upper right corner of Fig. 5.3. Since the mesh is fully symmetric, the mesh sizes h_i in the x-direction are displayed in the upper left corner.

It is observed that the mesh refined in a small local region. In fact, from Figs. 5.2 and 5.4, we note the fact that the spatial refinement has been restricted to the center of the whole domain where the solution develops singularity when t approaches the quenching time T. This indicates the efficiency of our adaptive process.

To compute more accurately the quenching time and view more clearly the quenching phenomena and the adaptive process, we may adopt an iterative stopping strategy. That is, where $u > 1 - \tau_{\min}$, we reduce the time step size $\tau_{\min}$ by half and continue the computation; when $u > 1 - \tau_{\min}/2$ we then reduce the time step to $\tau_{\min}/4$; repeat this fashion until a given number of such iterations are reached. Adopting this iterative stopping

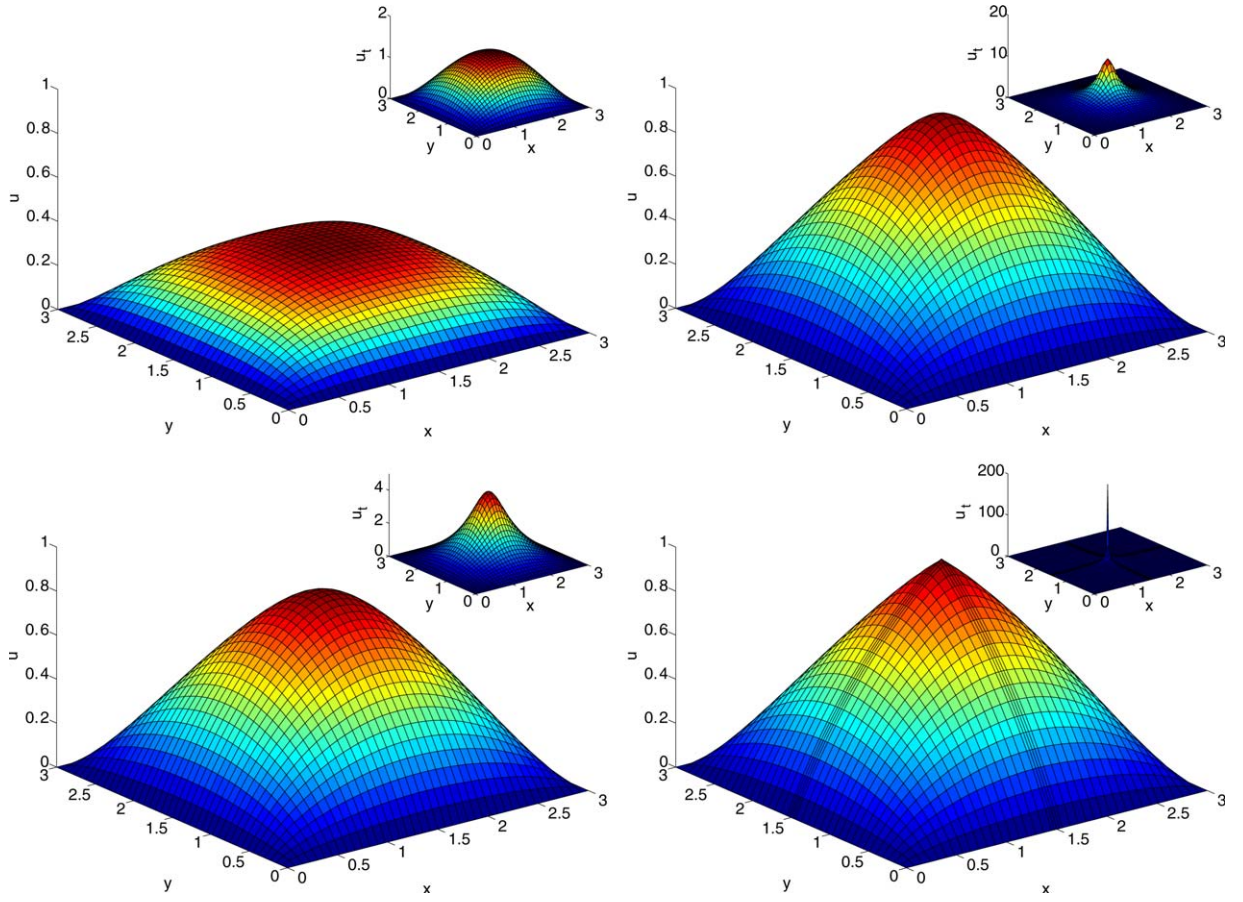

Fig. 5.2. The evolution profile of the functions u and u_t until immediately before quenching ($a = 3.0$, $a/b = 1$, $q = 0$, $\theta = 1$, $\tau_0 = 0.001$ and $\tau_{\min} = 1.0 \times 10^{-5}$). Left: from top to bottom, $t = 0.3$, 0.6; Right: from top to bottom, $t = 0.61402$, 0.61697. The derivative functions u_t are displayed as a sub-graphs.

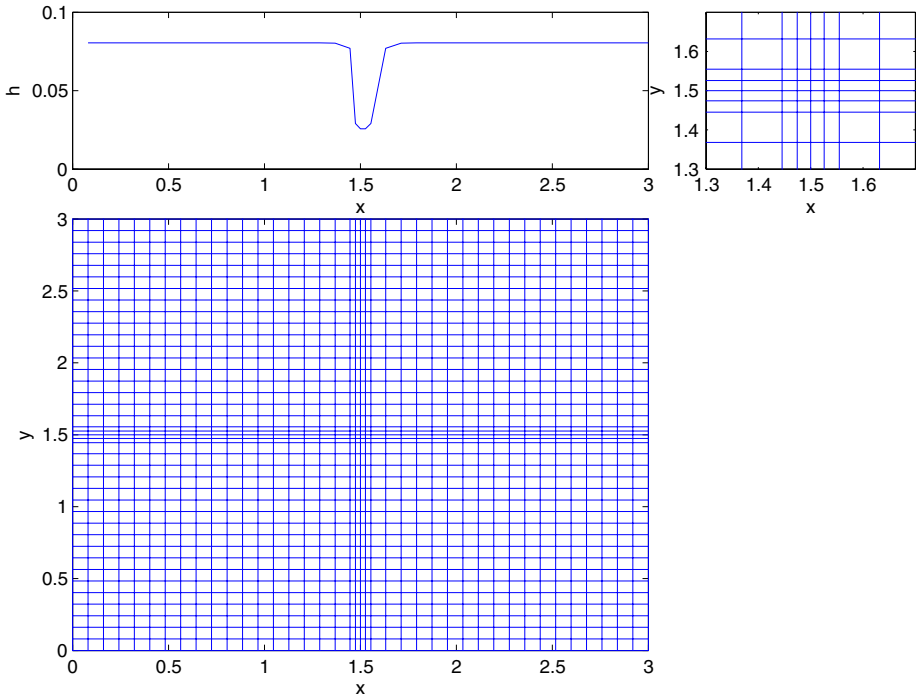

Fig. 5.3. The spatial adaptive mesh immediately before quenching at $t = 0.61697$ ($a = 3.0$, $a/b = 1$, $\theta = 1$, $\tau_0 = 0.001$ and $\tau_{\min} = 1.0 \times 10^{-5}$). The central part of the adaptive mesh is enlarged in the right sub-graph. Since the mesh is fully symmetric, the mesh sizes h_i only in the x-direction are displayed in the left sub-graph.

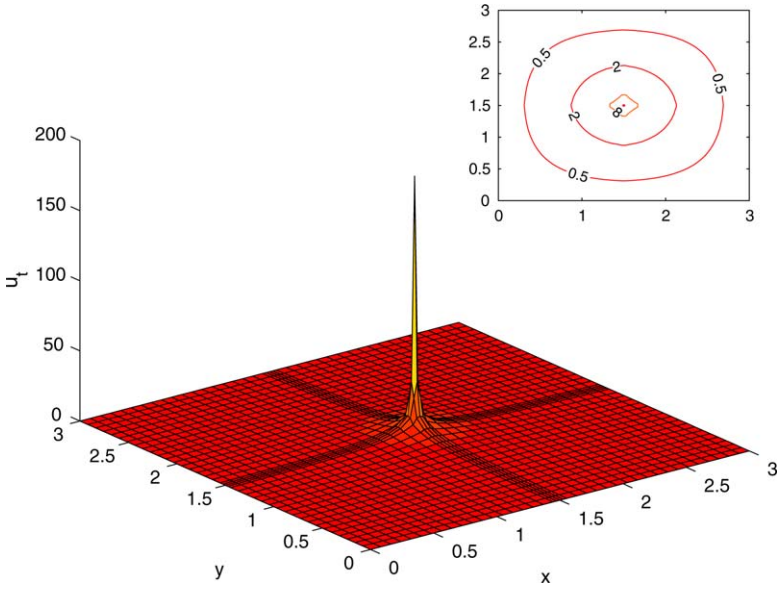

Fig. 5.4. The function u_t and its contour map immediately before quenching ($a = 3.0$, $a/b = 1$, $\theta = 1$, $\tau_0 = 0.001$, $\tau_{\min} = 1.0 \times 10^{-5}$ and time of plotting $t = 0.61697$). We note that the peak has reached 185.37580. A contour map of u_t is displayed as a sub-graph.

strategy more accurate solution is obtained and depicted in Fig. 5.5 (with 81×81 grid points). We may find evidently that the derivative function u_t will blow up soon since the peak of u_t reaches 3.1×10^9.

In Table 5.3, we consider the case of $\theta = 1.5$. Computational results about the critical sizes are listed for the different ratios of a/b.

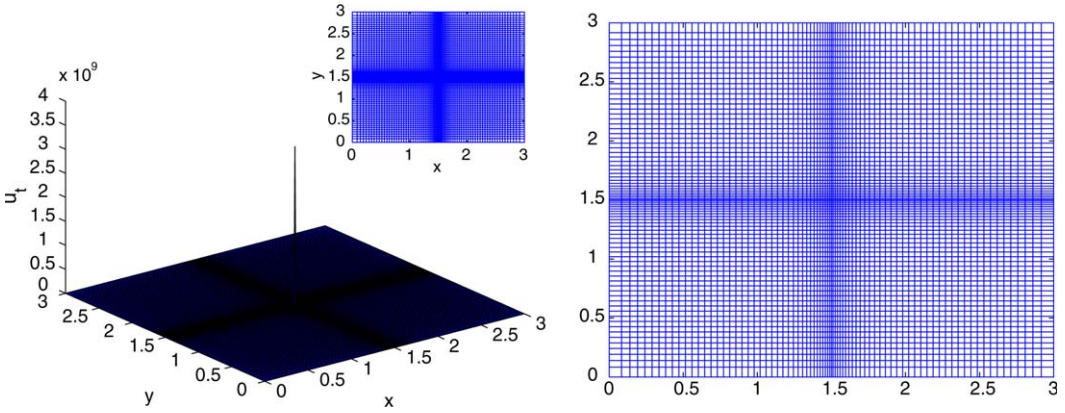

Fig. 5.5. The function u_t and its spatial adaptive mesh immediately before quenching ($a = 3.0$, $a/b = 1$, $\theta = 1$ and $N = 81 \times 81$). Left: Adopting the iterative stopping strategy the peak of u_t reaches 3.1×10^9. The spatial adaptive mesh immediately before quenching is displayed as a sub-graph. Right: The close-up look of the spatial adaptive mesh is depicted.

Table 5.3
Numerical prediction of the critical size and the quenching time in the case of $\theta = 1.5$

Ratio a/b	a	D
0.5	1.44995	4.20471
1.0	1.82999	3.34886

The number of spatial grids and initial temporal step size as well as minimal temporal controller are the same as those in Table 5.1.

In Fig. 5.6 we show the quenching rate, which was conjectured in Remark 4.1. We take the evolution of $\ln(1 - u(\frac{a}{2}, \frac{b}{2}, t))$ (Y-axis) as a function of $\ln(T - t)$ (X-axis), where $(\frac{a}{2}, \frac{b}{2})$ is the quenching point and T is the quenching time. The slope of the obtained curve approximately gives the quenching rate (conjectured as $\frac{1}{1+\theta}$). The slope in the left profile of Fig. 5.6 is $\frac{1}{2}$ when the problem (5.32), (5.34) with $\theta = 1$ is considered. Similarly, the slope in the right is $\frac{1}{4}$ when $\theta = 3$. Furthermore, we may estimate the constant of the quenching rate at the quenching point, that is, $(1 - u) = 1.2079(T - t)^{1/2}$ and $(1 - u) = 1.4129(T - t)^{1/4}$ for the case of $\theta = 1$ and $\theta = 3$ respectively. These results verify the conjecture that quenching rate may be $\frac{1}{1+\theta}$.

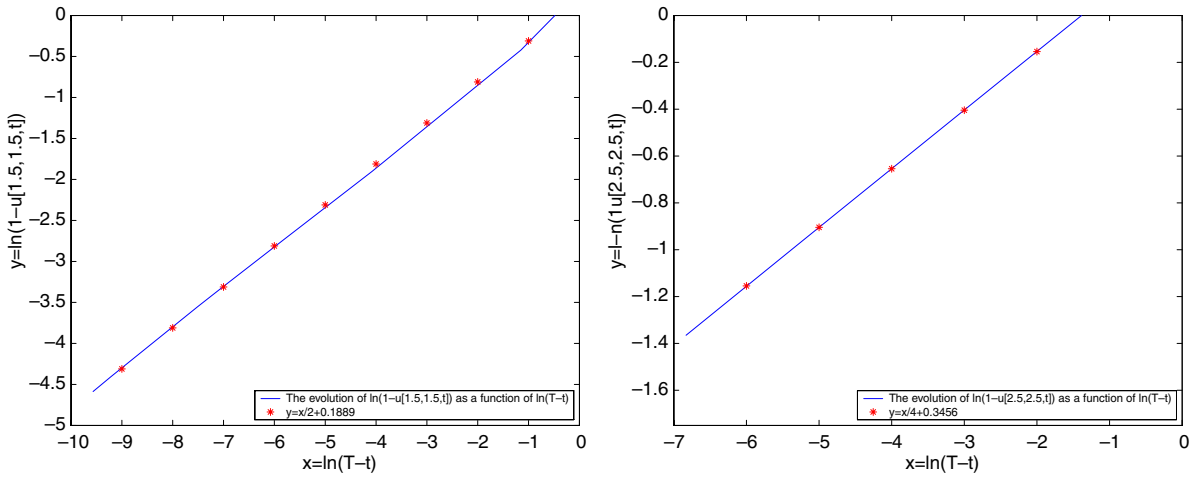

Fig. 5.6. The quenching rate for the problem (5.32), (5.34). The slope of the curve measures the quenching rate. And the line connecting the points is obtained by the least square approximation. Left: $a = 3.0$, $a/b = 1$ and $\theta = 1$; Right: $a = 5.0$, $a/b = 1$ and $\theta = 3$.

Example 5.2.2. Consider the degenerate quenching-combustion problem

$$\left(x^2+y^2\right)^{q/2}u_t = u_{xx}+u_{yy}+\frac{1}{(1-u)^{\theta}}, \quad (x,y)\in D,\ 0<t<T, \tag{5.35}$$

$$u(x,y,0)=0, \quad (x,y)\in D; \tag{5.36}$$

$$u(0,y,t)=u(a,y,t)=u(x,0,t)=u(x,b,t)=0, \quad 0<t<T. \tag{5.37}$$

where $q\neq 0$, $\theta>0$ and $D=(0,a)\times(0,b)$. Fig. 5.7 depicts a close-up look of the solution u and its derivative u_t immediately before quenching in the case of $q=1$. Since the effect of the coefficient $(x^2+y^2)^{q/2}$ in (5.35), the location of quenching point shifts slightly from the center to (1.34605,1.34605). This well agrees with the existing predictions given in earlier investigations [11] using uniform mesh and more grid points.

Example 5.2.3. We consider the vortex model of the type II superconductor. Under some conditions, the magnetic field develops a particular type of singularity, which is named a vortex (see [31,26] and therein references). In general, a vortex is not situated in a plane, but under some reasonable physical condition, the planar approximation is relevant and in this case, the physical model can be given as

$$u_t = u_{xx}+u_{yy}+\frac{1}{(1-u)^{\theta}}-\mathrm{e}^{-(1-u)}H_0, \quad (x,y)\in D,\ 0<t<T, \tag{5.38}$$

$$u(x,y,0)=0, \quad (x,y)\in D; \tag{5.39}$$

$$u(-a,y,t)=u(a,y,t)=u(x,-b,t)=u(x,b,t)=0, \quad 0<t<T. \tag{5.40}$$

where $D=(-a,a)\times(-b,b)$ and H_0 is the applied magnetic field assumed to be a constant. In this model, a vortex reconnection with the boundary, i.e., $1-u(x,y,t)=0$, means quenching. Actually, we may obtain (5.32), (5.34) by setting $H_0=0$ in (5.38), (5.40). Here we take $\theta=1$ and $H_0=1.0$.

Fig. 5.8 shows the profile of the solution u and its derivative u_t immediately before quenching at $t=0.77013$. Although the source function $f(u)$ in (5.38) has a different term $-e^{-(1-u)}H_0$ compared with one in (5.32), $\frac{1}{(1-u)^{\theta}}$ is still the dominant part in the source function, especially when $1-u$ approaches 0. So the profile of the solution u and its derivative u_t are similar as ones in (5.32), (5.34). However, the effect of $-e^{-(1-u)}H_0$ to the quenching rate can not be ignored. Similarly as the strategy in Fig. 5.6 we take the evolution of $\ln(1-u(0,0,t))$ (Y-axis) as a function of $\ln(T-t)$ (X-axis), where (0, 0) is the quenching point and T is the quenching time. In Fig. 5.9, the slope of the real line measures the quenching rate. And the dashed connecting the points is obtained by the least square approximation with the fixed slope 1/2. From Fig. 5.9 we observe that the slope of the quenching rate is tinily smaller than 1/2, which is the conjectured quenching rate $1/(1+\theta)$ for the case $H_0=0$. Such a tiny difference is reasonable due to the effect of the negative finite term $-\mathrm{e}^{-(1-u)}H_0$.

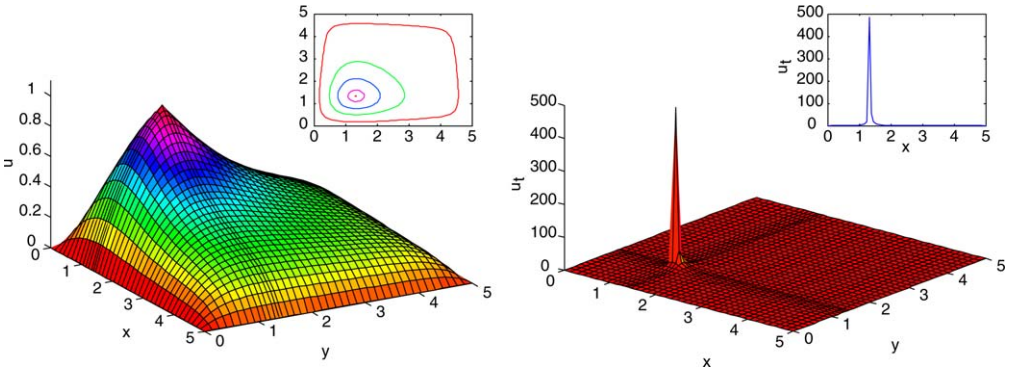

Fig. 5.7. The solution u and its derivative u_t of the problem (5.35), (5.37) immediately before quenching ($q=1$, $a=5.0$, $a/b=1$, $\theta=1$, $\tau_0=0.001$ and $\tau_{\min}=1.0\times10^{-5}$). Left: The solution u is displayed in the main figure when $t=1.22570$. The contour map of the numerical solution u is plotted as a sub-graph. Right: The derivative u_t is displayed in the main figure when $t=1.22570$. Projection of the function $\max_y u_t$ in x–u_t plane is given as a sub-graph.

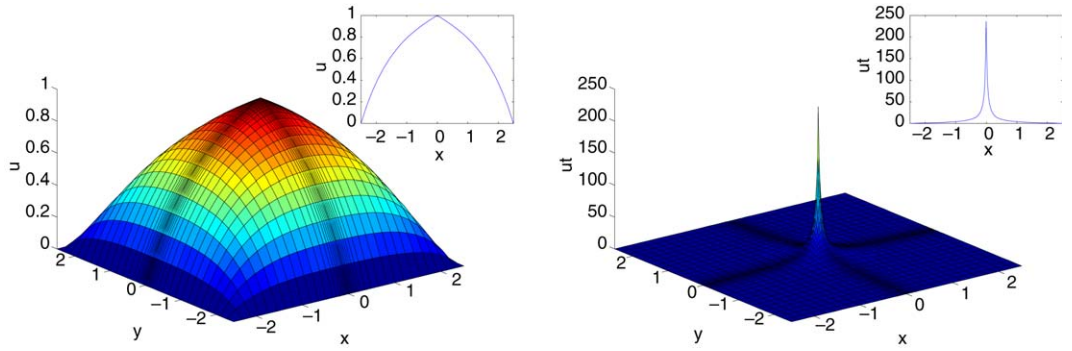

Fig. 5.8. The solution u and its derivative u_t of the problem (5.38)–(5.40) immediately before quenching ($a = 2.5$, $a/b = 1$, $\theta = 1$, $\tau_0 = 0.001$ and $\tau_{\min} = 1.0 \times 10^{-5}$). Left: The solution u is displayed in the main figure when $t = 0.77013$. Projection of the function $\max_y u$ in x–u plane is given as a sub-graph. Right: The derivative u_t is displayed in the main figure when $t = 0.77013$. Projection of the function $\max_y u_t$ in x–u_t plane is given as a sub-graph.

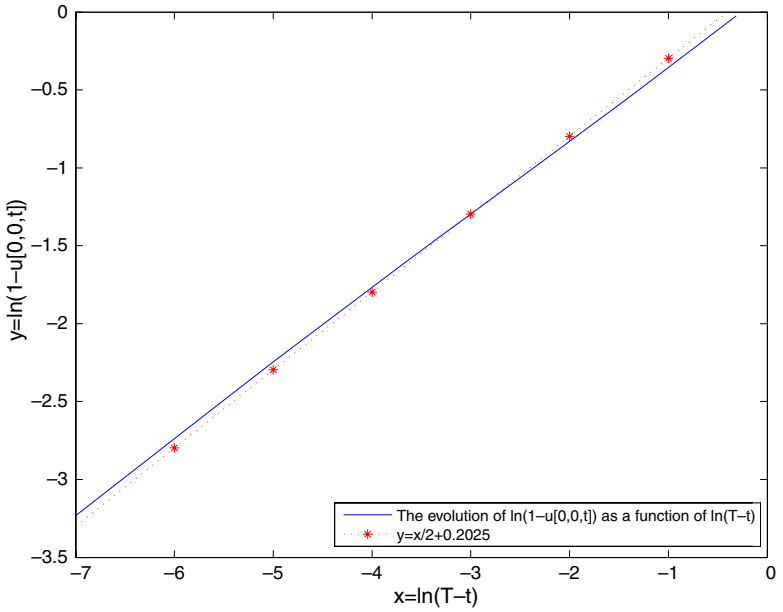

Fig. 5.9. The quenching rate for the problem (5.38)–(5.40) with $a = 2.5$, $a/b = 1$, $\theta = 1$ and $H_0 = 1.0$. The slope of the real line measures the quenching rate. And the dashed connecting the points is obtained by the least square approximation with the fixed slope 1/2.

6. Conclusion

In this paper we have applied a splitting moving mesh technique to a reaction–diffusion of quenching type. The adaptive method, based on a Peaceman–Rachford splitting of the original higher-dimensional model, is derived from a one-dimensional moving mesh technique using arc-length type of monitor function in terms of u_t (see (2.15) or (2.16)). The method may be seen as a special case of fully two-dimensional moving mesh method based on a minimization of a mesh-energy integral, but much simpler in implementation. In the monitor function (2.16), a time and solution dependent parameter α is chosen to be $|u_t|^{-1}$ automatically. Such a splitting moving mesh technique works well for the model problem with point singularities or defects. Due to the one-dimensional feature of our method analysis can be conducted relatively easily. The physical monotonicity of the solution can be proved for this algorithm under a special time marching implementation. Stability of the variable step moving mesh scheme is considered and a stability justification near the quenching

time is included. The good performance of the method for this quenching model is demonstrated through a number of quenching examples and a vortex model of type II superconductor. A parallel implementation of the splitting scheme incorporated with the mesh moving is also demonstrated through an example. Three or higher-dimensional problems can be implemented similarly.

Acknowledgements

The authors would like to thank the Institute of High Performance Computing (IHPC) for the support of this research work which was funded by the Grant: R-146-000-036-592. The authors would also like to thank anonymous referees for their valuable comments and suggestions.

References

[1] A. Acker, W. Walter, The quenching problem for nonlinear parabolic differential equations, in: Ordinary & Partial Differential EquationsLecture Notes in Mathematics, vol. 564, Springer-Verlag, New York and Berlin, 1976, pp. 1–12.
[2] A. Acker, B. Kawohl, Remarks on quenching, Nonlinear Anal. 13 (1989) 53–61.
[3] J.U. Brackbill, An adaptive grid with direction control, J. Comput. Phys. 108 (1993) 38–50.
[4] C.J. Budd, W. Huang, R.D. Russell, Moving mesh methods for problems with blow-up, SIAM J. Sci. Comput. 17 (1996) 305–327.
[5] W. Cao, W. Huang, R.D. Russell, A moving mesh method in multiblock domains with application to a combustion problem, Numer. Methods Partial Differential Equations 15 (1999) 449–467.
[6] W. Cao, W. Huang, R.D. Russell, A study of monitor functions for two-dimensional adaptive mesh generation, SIAM J. Sci. Comput. 20 (1999) 1978–1994.
[7] H. Ceniceros, T. Hou, An efficient dynamically adaptive mesh for potentially singular solutions, J. Comput. Phys. 172 (2001) 609–639.
[8] C.Y. Chan, Computation of the critical domain for quenching in an elliptic plate, Neural Parallel Sci. Comput. 1 (1993) 153–162.
[9] C.Y. Chan, L. Ke, Parabolic quenching for nonsmooth convex domains, J. Math. Anal. Appl. 186 (1994) 52–65.
[10] C.Y. Chan, P.C. Kong, Channel flow of a viscous fluid in the boundary layer, Quart. Appl. Math. 55 (1997) 51–56.
[11] H. Cheng, P. Lin, Q. Sheng, R.C.E. Tan, Solving degenerate reaction–diffusion equations via variable step Peaceman–Rachford splitting, SIAM J. Sci. Comput. 25 (2003) 1273–1292.
[12] J.M. Coyle, J.E. Flaherty, R. Ludwig, On the stability of mesh equidistribution strategies for time-dependent partial differential equations, J. Comput. Phys. 62 (1986) 26–39.
[13] J. Douglas Jr., J.E. Gunn, A general formulation of alternating direction methods I. Parabolic and hyperbolic problems, Numer. Math. 6 (1964) 428–453.
[14] M. Fila, J. Hulshof, A note on the quenching rate, Proc. Amer. Math. Soc. 112 (2) (1991) 473–477.
[15] M.S. Floater, Blow-up at the boundary for degenerate semilinear parabolic equations, Arch. Rat. Mech. Anal. 114 (1991) 57–77.
[16] R.M. Furzeland, J.G. Verwer, P.A. Zegeling, A numerical study of three moving-grid methods for one-dimensional partial differential equations which are based on the method of lines, J. Comput. Phys. 89 (1990) 349–388.
[17] J.-S. Guo, On the quenching rate estimate, Quart. Appl. Math. 49 (1991) 747–752.
[18] W. Huang, Y. Ren, R.D. Russell, Moving mesh partial differential equations (MMPDES) based on the equidistribution principle, SIAM J. Numer. Anal. 31 (1994) 709–730.
[19] W. Huang, R.D. Russell, Moving mesh strategy based on a gradient flow equation for two-dimensional problems, SIAM J. Sci. Comput. 20 (3) (1999) 998–1015.
[20] W.H. Hundsdorfer, J.G. Verwer, Stability and convergence of the Peaceman–Rachford ADI method for initial-boundary value problems, Math. Comput. 53 (187) (1989) 81–101.
[21] H. Kawarada, On solutions of initial-boundary value problems for $u_t = u_{xx} + 1/(1-u)$, Publ. Res. Inst. Math. Sci. 10 (1975) 729–736.
[22] B.I. Kvasov, Methods of Shape-Preserving Spline Approximation, World Scientific, Singapore, 2000.
[23] J. Lang, A. Walter, An adaptive Rothe method for nonlinear reaction–diffusion systems, Appl. Numer. Math. 13 (1993) 135–146.
[24] H.A. Levine, Quenching, nonquenching, and beyond quenching for solutions of some parabolic equations, Ann. Math. Pure Appl. 4 (1989) 243–260.
[25] H.A. Levine, Advances in quenching, in: Proceedings of the International Conference on Reaction–Diffusion Equations and Their Equilibrium States, Gregynog, Wales, August 1989.
[26] F. Merle, H. Zaag, Reconnection of vortex with the boundary and finite time quenching, Nonlinearity 10 (1997) 1497–1550.
[27] R. Li, T. Tang, P. Zhang, Moving mesh methods in multiple dimensions based on harmonic maps, J. Comput. Phys. 170 (2001) 562–588.
[28] H. Ockendon, Channel flow with temperature-dependent viscosity and internal viscous dissipation, J. Fluid Mech. 93 (1979) 737–746.
[29] D.W. Peaceman, H.H. Rachford Jr., The numerical solution of parabolic and elliptic differential equations, J. Soc. Indust. Appl. Math. 3 (1955) 28–41.
[30] M.H. Protter, H.F. Weinberger, Maximum Principles in Differential Equations, Prentice-Hall, Englewood Cliffs, NJ, 1967.
[31] Timo Salin, Quenching and blowup problems for reaction diffusion equations, Ph.D. Dissertation, Helsinki University of Technology Institute of Mathematics Research Reports, Helsinki University of Technology, 2004.

[32] M. Schatzman, Stability of the Peaceman–Rachford approximation, J. Funct. Anal. 162 (1999) 219–255.
[33] Q. Sheng, Exponential splitting methods for partial differential equations, Ph.D. Dissertation, DAMTP, Cambridge University, 1990.
[34] Q. Sheng, A monotonically convergent adaptive method for nonlinear combustion problems, in: Integral Methods in Science & EngineeringResearch Notes in Mathematics, 418, Chapman & Hall/CRC, London and New York, 2000, pp. 310–315.
[35] J. Stoer, R. Bulirsch, Introduction to Numerical Analysis, Springer, New York, 1993.
[36] P.A. Zegeling, Tensor-production adaptive grids based on coordinate transformations, J. Comput. Appl. Math. 166 (2004) 343–360.